Journal of Pharmaceutical and Biomedical Analysis 53 (2010) 7–14

Contents lists available at ScienceDirect

Journal of Pharmaceutical and Biomedical Analysis

journal homepage: www.elsevier.com/locate/jpba

Modelling phase transition kinetics of chenodeoxycholic acid with the Runge–Kutta method

Sanita Petkune*, Andris Actins

University of Latvia, The Faculty of Chemistry, Kr. Valdemara Street 48, Riga LV-1013, Latvia

ARTICLE INFO

Article history:
Received 30 October 2009
Received in revised form 24 February 2010
Accepted 26 February 2010
Available online 6 March 2010

Keywords:
Chenodeoxycholic acid
Drug polymorphism
Kinetics of polymorphs
X-ray diffraction
Runge–Kutta method

ABSTRACT

The phase transition kinetics of two chenodeoxycholic acid polymorphic modifications—*form I* (stable at high temperature), *form III* (stable at low temperature) and the amorphous phase has been examined under various conditions of temperature and relative humidity. *Form III* conversion to *form I* was examined at high temperature conditions and was found to be non-spontaneous, requiring seed crystals for initiation. The formation kinetic model of *form I* was created incorporating the three-dimensional seed crystal growth, the phase transition rate proportion to the surface area of *form I* crystals, and the influence of the amorphous phase surface area changes with an empirical stage pointer q that contained the incomplete transition of the amorphous phase to *form I* with a residue ω_{A_∞}. The extent of transition and the phase transition rate constant depended on *form I* seed crystal amount in the raw mixture, and on the sample preparation. To describe phase transition kinetic curves, we employed the Runge–Kutta differential equation numeric solving method. By combining the Runge–Kutta method with the multi-point optimization method, the average quadratic deviation of the experimental results from one calculated series was under 2%.

1. Introduction

The need to control polymorph formation has been an important issue in the chemical industry for over a century because many pharmaceutically active ingredients can exist in several different crystalline forms. The term polymorphism has come to denote those crystal systems for which a substance can exist in two or more crystalline phases with different unit cells, but where each of the forms has the same elemental composition [1]. Since polymorphs have different lattice energy and entropy, there are significant differences in their physical properties that have an important effect on the processing of drug substances into drug products [2]. Therefore, solid-state physical and chemical stability has a significant impact on the quality, safety, and shelf life of drug substances and drug products, and it is important to control the crystal form of the drug substance during various stages of manufacturing [1].

Quantitative solid-state analysis and investigation of polymorphic transition kinetics under various controlled storage conditions are needed to ensure that the polymorphic composition remains within accepted limits throughout the self-life of a drug product [3]. The thermodynamic stability region may be defined with a phase diagram of polymorphic forms, which represents the dependence between equilibrium pressure p/p_o and temperature of polymorphic transitions. Conversely, for determining the equilibrium pressure, it is necessary to find the phase transition rate constant dependence on pressure at fixed temperature. For this purpose, it is essential to find a suitable kinetic model for the phase transition.

Chenodeoxycholic acid (3α,7α-dihydroxy-5β-cholanic acid, CDCA, Fig. 1) is one of the major bile acids in humans and some animals. Therapeutic uses of CDCA include the treatment of gallstone disease [4]. Three CDCA polymorphic *forms I*, *II* and *III*, have been reported [5], with melting temperatures of 168, 138 and 119 °C, respectively. *Form III* is obtained by crystallization of CDCA from an ethylacetate or chloroform solution [6], followed by the removal of solvent residues from solvate crystals, and this form may be a desolvated isostructural solvate [7]. CDCA high temperature *form I* has monoclinic unit cell with $a = 18.785(14)$ Å, $b = 8.120(6)$ Å, $c = 14.889(11)$ Å, $\beta = 99.10(2)^\circ$ and $Z = 4$ and space group $P2_1$ [8]. The low temperature *form III* belongs to the hexagonal system with space group $P6_5$ and its unit cell parameters are $a = 22.250(5)$ Å, $c = 10.255(2)$ Å, $Z = 6$, $V = 4396.7$ Å^3 [9]. Crystallographic data could not be found for the *form II*. The form in pharmaceutical use, which is available as a certified reference standard, appears to be amorphous by X-ray diffraction analysis.

In order to characterize the solid forms, a variety of physical techniques are employed. These techniques rely on differences of atom arrangement in crystals (X-ray diffraction), energies of bond

* Corresponding author. Tel.: +371 29485081.
E-mail address: sanitapetkune@yahoo.com (S. Petkune).

0731-7085/$ – see front matter © 2010 Elsevier B.V. All rights reserved.
doi:10.1016/j.jpba.2010.02.038

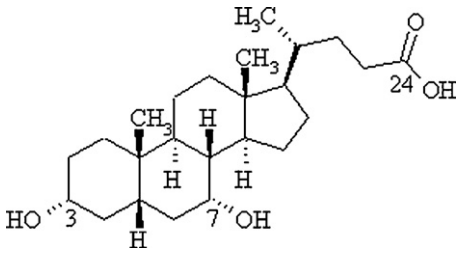

Fig. 1. The chemical structure of chenodeoxycholic acid.

stretching/bending vibrations and lattice vibrations (infrared and Raman spectroscopy), electronic environments of nuclei (nuclear magnetic resonance), heat flow or weight change (thermal analysis) and morphology (optical microscopy) [10].

The purpose of this study was to investigate the phase transition dynamics of CDCA under various conditions of temperature and relative humidity, as well as to create the kinetic model for the transition to the thermodynamically stable *form I*. To describe phase transition kinetic curves, the Runge–Kutta differential equation was solved numerically. Phase ratios in the investigated CDCA samples were determined with X-ray powder diffractometric (PXRD) analysis.

2. Materials and methods

2.1. Materials

CDCA *form I* with 98+% purity was purchased from *Acros Organics* chemical company. All the solvents used were of analytical grade.

2.2. Preparation of CDCA polymorphs

CDCA *form III* was prepared by crystallization of *form I* from ethylacetate or acetone.

The X-ray amorphous phase of CDCA (further in the text—amorphous phase) was obtained by mechanically amorfizing (grinding in a mortar) of *form III* for about 60–70 min.

Commercial CDCA was a mixture of the amorphous phase and *form I*. Pure *form I* was obtained by heating the sample in a 3–5 mm thick layer at 130 °C for 15 h, or by heating a suspension of the amorphous phase or *form III* in cyclohexane at 75–80 °C for 12–24 h.

2.3. Preparation of samples for phase transition kinetic studies

Mixtures containing different proportions of CDCA *form I* and *form III* were prepared. The weight fractions of *form I* were 5%, 23% and 60%. Each mixture had a total weight of approximately 0.5 g. Mixtures were homogenized by grinding in a mortar for 2 min to reduce the variation in particle size.

Mixtures containing different proportions of *form I* and the amorphous phase were prepared. The weight fractions of *form I* in the mixtures with the amorphous phase were 1%, 2%, 3%, 5%, 10%, 20%, 30%, 50% and 60%. Mixtures were homogenized by grinding in a mortar for 2 min. Mixtures containing 2% of *form I* were homogenized by grinding in a mortar for 1.0, 1.5, 2.5 and 5.0 min, or by shaking in a *Retsch MM 300* shaker (Retsch GmbH, Germany) with the shaking frequency 7 s^{-1} for 2.0 and 5.0 min.

2.4. Polymorph characterization methods

2.4.1. Powder X-ray diffractometry (PXRD)

Powder XRD measurements were performed on a *Bruker D8 Advance* diffractometer (Bruker AXS, Karlsruhe, Germany). The divergence and scattering slits were set at 1.0 mm, and the receiving slit was set at 0.6 mm. Diffraction patterns within the 2θ range of 3–30° were recorded at room temperature using CuK_α radiation at a 1.54180 Å wavelength with the following measurement conditions: tube voltage of 40 kV, tube current of 40 mA, step-scan mode with the step size of 0.02° 2θ and counting time of 0.5 s/step. Powder samples were packed into glass holders with a weight capacity of 150 mg; the sample surface was flattened with a spatula and glass slide to ensure coplanarity of the powder surface with the surface of the holder and to minimize preferred orientation effects. Diffractograms were analyzed with *DIFRAC^{plus} EVA* (ver. 12.0) diffraction software.

2.4.2. Differential scanning calorimetry (DSC)

DSC analysis was performed on a *METTLER TOLEDO 823e DSC* (Mettler Toledo, Switzerland) instrument operating with the version 9.0 of Star^e Software. The measurements were made using 4–6 mg samples in aluminium pans at a heating rate of 10 °C/min over the temperature range of 35–180 °C. Transition temperatures and melting points were determined as the intersection point between the base line and the linear section of the ascending endothermic curve.

2.4.3. Thermal gravimetric analysis (TGA)

TGA analysis was performed on 8–10 mg samples with an *EXSTRAR 6000 TG/DTA 6300* (Seiko, Japan) analyzer at a heating rate of 10 °C/min over the temperature range of 30–180 °C.

2.4.4. Infrared (IR) spectroscopy

IR spectra were recorded on an *ATI FTIR FM* (ATI MATTSON, Madison, WI) spectrophotometer over the range of 4000–400 cm^{-1} in KBr pellets. Approximately 1 mg of sample was mixed with 400 mg of KBr by means of an agate mortar and pestle, and a 100 mg tablet of this mixture was made by a GRASEBY SPECAL press. The background was collected in the same range for air. Analytical grade KBr from *Acros Organics* was used for IR spectroscopy.

2.5. Phase transition kinetic studies

Observations of CDCA *form I* and *form III* phase transition kinetics were performed at 80, 90, 95, 100 and 110 °C, using mixtures of *form I* and *form III* containing 10% weight fraction of *form I* seed crystals in the raw mixture.

Similarly, phase transition kinetics of *form I* and *form III* were investigated at 95 °C using mixtures of *form I* and *form III* containing 5%, 10%, 23% and 60% weight fraction of *form I* seed crystals.

Phase transition kinetic study of the CDCA amorphous phase and *form I* was performed at 95 °C using mixtures of the amorphous phase and *form I* containing 1%, 2%, 3%, 5%, 10%, 20%, 30%, 50% and 60% weight fraction of *form I* seed crystals.

Phase transition kinetics of the CDCA amorphous phase and *form I* was studied at 50 °C under high relative humidity (RH): 74%, 83%, 95% and 100% RH using mixtures containing 2% weight fraction of *form I* seed crystals.

Depending on transformation rate, after fixed time PXRD data were recorded.

2.5.1. Control of relative humidity

To obtain the stable relative humidities of 74%, 83% and 95%, sulphuric acid solutions of concentrations, 30%, 23% and 10% were used, respectively. Pure water provided the relative humidity of 100%.

2.5.2. Temperature control

Desiccators with sulphuric acid solutions were put in an air thermostat at 50 ± 1 °C for 24 h before CDCA sample insertion.

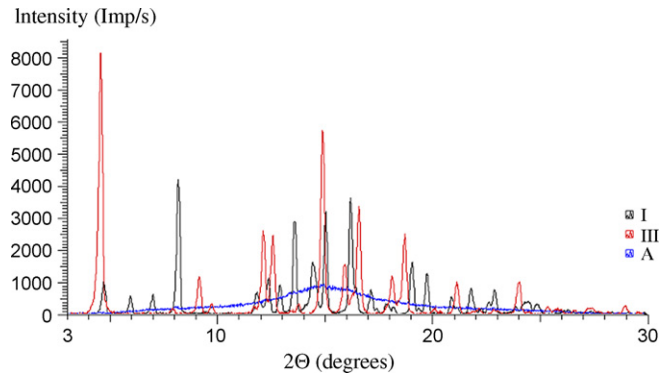

Fig. 2. Powder X-ray diffraction patterns of CDCA high melting *form I*, the low melting *form III* and the amorphous phase A.

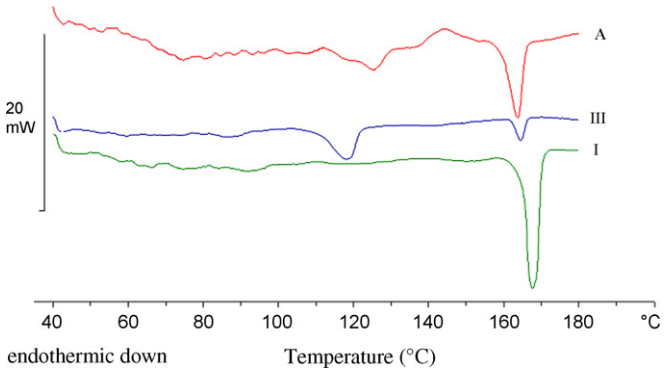

Fig. 3. DSC profiles of CDCA *form I* (1), *form III* (2) and the amorphous phase (3).

2.6. Quantitative analysis

Determination of polymorph quantitative content was carried out with *DIFRAC*^{plus} *EVA* (ver. 12.0) diffraction software.

In mixtures of CDCA polymorphs (*form I* and *form III*, amorphous phase and *form I*) one of the polymorphs is considered as the "unknown" component whilst another is the matrix. For example, in a phase transition kinetic study of the amorphous phase and *form I*, the basic relationship (Eq. (1)) used in quantitative analysis involving PXRD is as follows [11]:

$$Ii_I = \frac{K\omega_I}{p_I \mu_A^*} \quad (1)$$

Ii_I is the intensity of line i of *form I*; K is the constant; ω_I is the weight fraction of *form I*; p_I is the density of *form I*; μ_A^* is the mass absorption coefficient of the amorphous phase.

In a sample containing 100% of *form I*, the intensity of line i, represented by $(Ii_I)_o$, can be determined using Eq. (2), where μ_I^* is the mass absorption coefficient of *form I*.

$$(Ii_I)_o = \frac{K}{p_I \mu_I^*} \quad (2)$$

Since the mass absorption coefficient values to the polymorphs of one compound are the same, the *form I* content in the mixture with the amorphous phase can be determined using Eq. (3):

$$\frac{Ii_I}{(Ii_I)_o} = \omega_I \quad (3)$$

Using Eq. (3), a plot of intensity ratio $Ii_I/(Ii_I)_o$ against the weight fraction of *form I* (ω_I), should give a straight line with a slope 1.

3. Results and discussion

3.1. Solid-state characterization of polymorphs

CDCA polymorphic forms were identified using PXRD, DSC and IR spectroscopy. The PXRD (Fig. 2) patterns of polymorphs *I* and *III* had unique peaks that can be used for their identification and quantitative determination. The characteristic peaks of *form I* were observed at 5.9°, 7.0°, 8.1°, 13.0°, 19.1° (2Θ), while those of *form III* were observed at 4.5°, 9.1°, 15.8°, 18.6° (2Θ). The quantitative analysis was performed using these peak intensities of both forms.

The DSC profiles of CDCA polymorphs *I*, *III* and the amorphous phase are shown in Fig. 3. The DCS curve of *form I* only exhibited an endothermic peak at 164.4–169.8 °C with a leading edge of 166.8 °C due to the melting. *Form III* showed an endotherm at 110.5–121.7 °C with a leading edge of 117.8 °C, corresponding to the melting of *form III* and to the crystallization of a small amount of *form I* from the melt, which in turn further melts at 161.9–166.2 °C with a leading edge of 164.2 °C. In the DSC curve there is no visible *form I* crystallization exotherm, because *form I* crystallizes in small quantity, as evidenced by the small *form I* melting endotherm, if it is compared with the pure *form I* melting endotherm. The amorphous phase exhibited an endothermic peak at 117.3–129.2 °C with a minimum at 124.6 °C due to the glass transition followed by an exotherm at 134.7–153.3 °C with a maximum at 144.0 °C, corresponding to the crystallization of *form I*. *Form I* further melts at 155.2–166.9 °C with a leading edge of 161.1 °C.

The TGA analysis of *form I* did not show any weight loss in the temperature range of 30–110 °C, while there was 0.6–1.1% weight loss for *form III*, indicating the presence of a small amount of solvent or adsorbed water.

To investigate the molecular state of CDCA polymorphs, FT-IR spectroscopy was carried out, and the results are shown in Fig. 4. Both polymorphic forms and the amorphous phase indicated an absorbance band due to C–O stretching vibrations in the region of 1074–1078 cm^{-1} and two weak absorbance bands due to C–H bending vibrations in the region of 1448–1470 cm^{-1}. All the forms also exhibited a strong absorbance band in the region of 1702–1714 cm^{-1} due to C=O stretching vibrations, and strong C–H aliphatic stretching vibration bands in the region of 2866–2933 cm^{-1}. The OH– stretching vibrations were observed as sharp bands at 3577, 3534 and 3394 cm^{-1} for the *form I*, at 3451 and 3307 cm^{-1} for the *form III* and at 3426 cm^{-1} for the amorphous phase.

Other authors have reported that the *form I* crystals contain two non-equivalent molecules of CDCA in the crystal lattice, and these molecules were approximately perpendicular to one another [8–9].

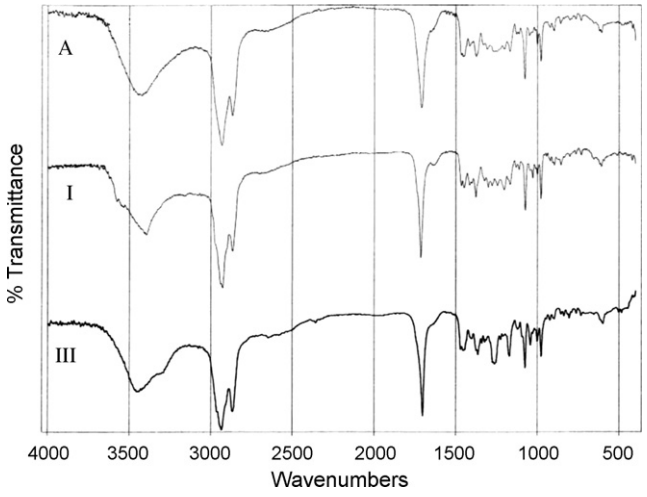

Fig. 4. IR spectra of CDCA *I* (1), *form III* (2) and the amorphous phase (3).

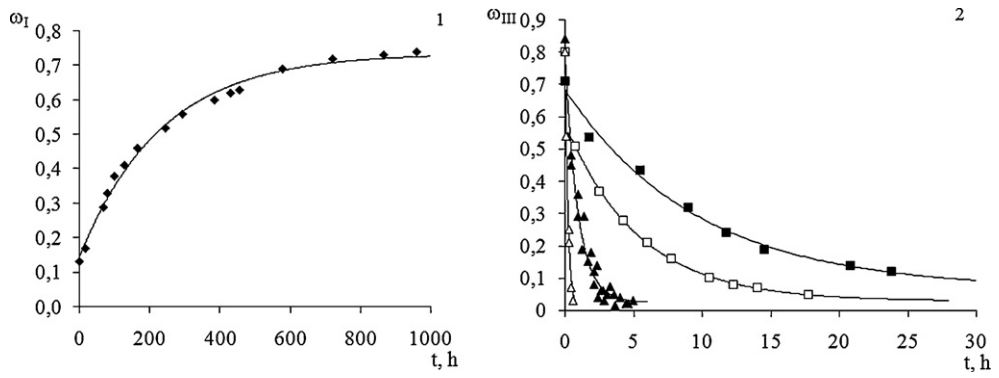

Fig. 5. The phase transition kinetic curves of *form III* and *form I* at 80 °C with 10% weight fraction of *form I* seed crystals in the raw mixture, $\omega_{I,teor} = 0.736 - (0.736 - 0.146)e^{-0.00427t}$ (1); the phase transition kinetic curves of *form III* amorfization at 90 °C (■), 95 °C (□), 100 °C (▲), 110 °C (△) (2).

Between the adjacent molecules A, the adjacent molecules B, and between the molecules A and B hydrogen bonds exist, forming a double sheet structure with tight packing. Those studies concluded that the *form III* crystal hydrogen bond network was not as extensive as that in the *form I* crystals and the *form III* crystals form a hexagonal channel type structure. The differences in OH– stretching vibration bands between *form I* and *form III* crystals are indicative of different hydrogen bond configurations in these crystal structures.

3.2. Phase transition kinetic studies

At the first stage of our investigation we established that the *form I* was thermodynamically stable throughout the temperature range of 25–168 °C. In addition, pure *form III* was kinetically stable at 25 °C, while slow amorphization was observed during isothermal heating for several days at temperatures up to 110 °C. It was observed as the decrease of peak intensities and the increase of the diffusive dispersion maximum intensity in the diffraction pattern. The transition of *form III* to the amorphous phase (A) was irreversible. Despite adding seed crystals of *form I* in *form III* samples to create crystallization centres, the transition of *form III* to *form I* was not observed at 60 °C, but at 80 °C the observed transition was slow. The kinetic curves of *form I* and *form III* mixtures initially containing 10% weight fraction of *form I*, exhibited an exponential nature at 80 °C (Fig. 5-1), therefore the *form III* to *form I* transition could be described with an empirical Eq. (4):

$$\omega_{I,teor} = \omega_{I_\infty} - (\omega_{I_\infty} - \omega_{I_o})e^{-kt} \quad (4)$$

where $\omega_{I,teor}$ is the theoretically calculated weight fraction of *form I*; ω_{I_∞} is the final weight fraction of *form I* when the phase transition has ceased; ω_{I_o} is the weight fraction of *form I* when $t = 0$; k is the phase transition rate constant, h^{-1}; t is the time, h.

The optimal k, ω_{I_∞} and ω_{I_o} values were determined by finding the minimal value of the goal function (5) using *MS Excel Solver* software.

$$S^2 = \sum_{i=1}^{n}[(\omega_{I_{teor}})_i - (\omega_{I_{eksp}})_i]^2 \quad (5)$$

When the mixture of *form I* and *form III* in a ratio 9:1 was heated at a temperature higher than 80 °C, the kinetic curves had a different nature (Fig. 6). Initially we tried to describe the kinetic transitions with kinetic equations from the literature [12–14] for the most common mechanism of solid-state reactions (Table 1).

For describing the transition kinetic process of *form I* and *form III*, two-dimensional (A2) and three-dimensional (A3) mechanisms of the crystal growth offered the best fit, but the compatibility of those mechanisms with experimental results was not entirely satisfactory. Therefore we developed a new kinetic model, based on the three-dimensional growth of *form I* seed crystals, where the phase transition rate was proportional to the surface area of *form I* crystals. We accounted for the influence of the amorphous phase surface area changes on the *form I* seed crystal formation and the *form I* growth rate. During the first hours, the content of *form III* decreased rapidly, but after that, the decrease of *form III* content could be best described by an exponential dependence on time. Probably *form III* first amorphized, removing solvent residues, because, as it is known [6], *form III* easily includes solvent molecules in the crystal structure channels. Apparently, the *form III* transition to *form I* proceeded through the formation of the amorphous phase (A) as

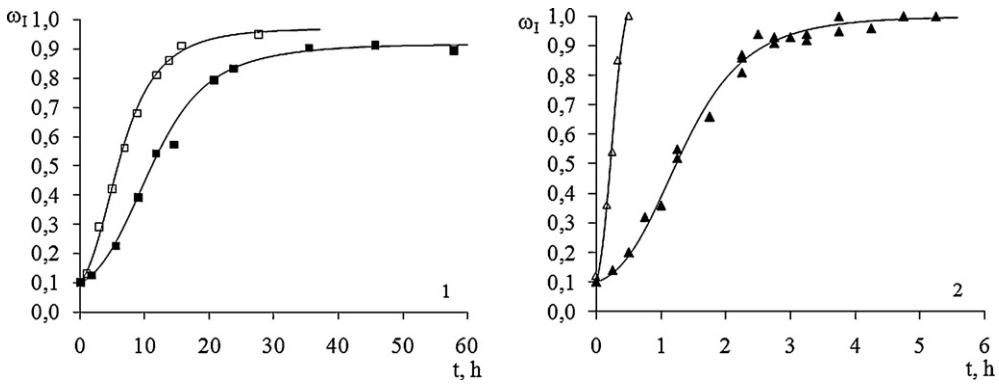

Fig. 6. The phase transition kinetic curves of *form III* and *form I* at 90 °C (■) and 95 °C (□) (1); at 100 °C (▲) and 110 °C (△) (2) with 10% weight fraction of *form I* seed crystals in the raw mixture.

Table 1
Kinetic equations for the most common mechanism of solid-state reactions.

Symbol	Equation	Mechanism
R1	$x = kt$	One-dimensional phase-boundary mechanism (zero-order mechanism)
R2	$(1-(1-x))^{1/2} = kt$	Two-dimensional phase-boundary mechanism (zero-order mechanism)
R3	$(1-(1-x))^{1/3} = kt$	Three-dimensional phase-boundary mechanism (spherical mechanism)
F1	$-\ln(1-x) = kt$	Random nucleation mechanism (first-order mechanism)
A2	$(-\ln(1-x))^{1/2} = kt$	Two-dimensional growth of nuclei mechanism (Avrami–Erofeev equation)
A3	$(-\ln(1-x))^{1/3} = kt$	Three-dimensional growth of nuclei mechanism (Avrami–Erofeev equation)
D1	$x^2 = kt$	One-dimension diffusion mechanism
D2	$(1-x)\ln(1-x)+x = kt$	Two-dimension diffusion mechanism
D3	$(1-(1-x)^{1/3})^2 = kt$	Three-dimension diffusion mechanism (Jander equation)
D4	$(1-2x/3)-(1-x)^{2/3} = kt$	Three-dimension diffusion mechanism (Ginstiling–Brounshtein equation)

an intermediate product:

$$form\ III \rightarrow A \rightarrow form\ I$$

A phase transition kinetic model was developed, considering each transition (*form III* → *A* and *A* → *form I*) separately.

3.2.1. The kinetic model of form III amorfization

Rapid changes of *form III* content in the kinetic description were considered as a correction of beginning conditions and the kinetics of the following slower process were analyzed (Fig. 5-2). The *form III* amorfization can be described with the empirical Eq. (6):

$$\omega_{III,teor} = \omega_{III_\infty} + (\omega_{III_o} - \omega_{III_\infty})e^{-k_1 t} \quad (6)$$

where $\omega_{III,teor}$ is the theoretically calculated weight fraction of *form III*; ω_{III_∞} is the final weight fraction of *form III* when the phase transition has ceased; ω_{III_o} is the initial weight fraction of *form III* when $t = 0$; k_1 is the phase transition rate constant, h^{-1}; t is the time, h; k_1, ω_{III_∞}, ω_{III_o} is the optimized values.

Calculated kinetic curves at 90, 95, 100 and 110 °C are shown in Fig. 5-2. We established that the rate constant of *form III* amorfization k_1 at 90 °C was 0.122 h^{-1}, at 95 °C it was 0.321 h^{-1}, at 100 °C it was 1.061 h^{-1}, and at 110 °C it was 4.673 h^{-1}. The optimized values are shown in Table 2. If the natural logarithm of the rate constant $\ln(k_1)$ is plotted against $1/T$, the activation energy can be calculated via the Arrhenius law: $\ln(k) = -(E_a/R)\cdot 1/T + \ln A$. An Arrhenius plot of $\ln k_1 - 1/T$ yielded a straight line with a slope of $-E_a/R$, and the activation energy of *form III* amorfization was found to be 210 kJ/mol.

3.2.2. The kinetic model of form III and form I phase transition.

The decrease of *form III* and the amorphous phase over time can be described with Eqs. (7) and (8).

$$\frac{d\omega_{III}}{dt} = k_1(\omega_{III_o} - \omega_{III_\infty})e^{-k_1 t} \quad (7)$$

$$\frac{d\omega_A}{dt} = -\frac{d\omega_{III}}{dt} - k_2\omega_I^p(\omega_A - \omega_{A_\infty})^q \quad (8)$$

and

$$\omega_A = 1 - \omega_{III} - \omega_I \quad (9)$$

Combining Eqs. (7)–(9), the following expression (10) is obtained which describes the time dependence of *form I* growth:

$$\frac{d\omega_I}{dt} = k_2\omega_I^p(1 - \omega_{III} - \omega_I - \omega_{A_\infty})^q \quad (10)$$

where ω_{III} is the weight fraction of *form III* at time t; ω_{III_∞} is the final weight fraction of *form III* when the phase transition has ceased; ω_{III_o} is the initial weight fraction of *form III* when $t = 0$; k_1 is the rate constant of *form III* amorfization, h^{-1}; ω_I is the weight fraction of *form I* at time t; ω_A is the weight fraction of the amorphous phase at time t; ω_{A_∞} is the weight fraction of the amorphous phase when the phase transition has ceased; k_2 is the phase transition rate constant of the amorphous phase transition to *form I*, h^{-1}; t is the time, h; q, p are the constants; k_1, ω_{III_∞}, ω_{III_o} constants were defined during the discussion of *form III* transition to the amorphous phase; k_2, ω_{III_o}, p, q are the optimized values.

The constant p characterizes the model of the crystal growth—if the growth is two-dimensional, $p = 1/2$, if three-dimensional, $p = 2/3$. However, the absolute modeling of such systems is difficult, because it is hard to choose the appropriate crystal growth model. The constant q represents the empirical exponential factor, which characterizes the influence of the amorphous phase surface area changes to the *form I* growth rate. It contains the incomplete transition of the amorphous phase to *form I* with the residue ω_{A_∞}.

For the differential Eq. (12) an analytical solution could not be obtained, therefore it was solved numerically using the Runge–Kutta differential equation solving method in the *MS Excel* software. The numeric method was based on a two-step differential scheme with the right-hand side function $f(t,x)$ multi-step recalculation, moving from the nth time step to the $(n+1)$th time step. If a sufficiently small time interval Δt was selected, the weight fraction of *form I* at the $(n+1)$th time step could be calculated:

$$\omega_{In+1} = \omega_{In} + \Delta\omega_I \quad (11)$$

where ω_{In} is the weight fraction of *form I* at the beginning of the time interval Δt; ω_{In+1} is the weight fraction of *form I* at the end of the time interval Δt; $\Delta\omega_I$ is the growth of *form I* during the time interval Δt.

In some cases the Runge–Kutta exponential operation was incompatible with the optimization software and there was a risk of producing negative constant values in the calculations. If in the $(n+1)$th time step values $w(A)$ and $\Delta w(A)$ were <0, the value of nth time step was attributed to the function.

Table 2
Optimized constant values of *form I* and *form III* phase transition kinetic curves at 90, 95, 100 and 110 °C containing 10% weight fraction of *form I* seed crystals in the raw mixture.

Temperature, °C	k_1, h^{-1}	ω_{III_o}	ω_{III_∞}	ω_{A_∞}	k_2, h^{-1}	q	p
90	0.12	0.74	0	0.089	0.40	1.03	0.67
95	0.20	0.74	0.031	0	0.87	1.34	0.67
100	0.99	0.74	0	0	2.55	0.90	0.67
110	6.04	0.74	0	0	10.3	0.70	0.67

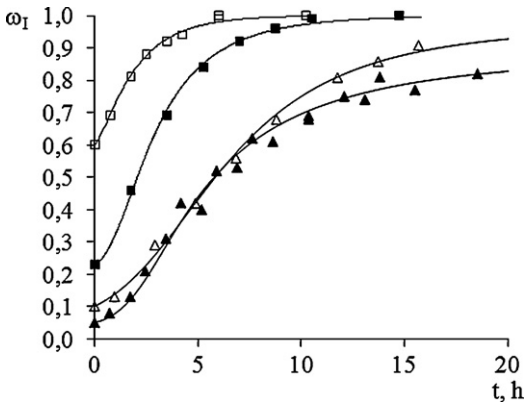

Fig. 7. The phase transition kinetic curves of *form III* and *form I* at 95 °C with 5% (▲), 10% (△), 23% (■) and 60% (□) weight fraction of *form I* seed crystals in the raw mixture.

Table 3
Optimized constant values of *form I* and *form III* phase transition kinetics curves at 95 °C.

ω_I in the raw mixture	k_1, h^{-1}	ω_{III_o}	ω_{III_∞}	ω_{A_∞}	k_2, h^{-1}	q	p
0.05	0.18	0.64	0.077	0	1.99	2.17	0.67
0.10	0.20	0.74	0.031	0	0.87	1.34	0.67
0.23	0.42	0.67	0	0	2.28	1.39	0.67
0.60	0.55	0.33	0	0	3.68	1.22	0.67

Kinetic curves for mixtures initially containing 10% weight fraction of *form I* were obtained at 90, 95, 100 and 110 °C (Fig. 6), with the optimized constant values listed in Table 2.

Since the transition from *form III* to *form I* occurred comparatively rapidly at 100 and 110 °C, but slowly at 90 °C, we selected 95 °C as the optimal temperature for phase transition kinetic studies using variable amounts of *form I* seed crystals in the raw mixture. Phase dynamic curves were obtained for the 5–60% range of *form I* weight fractions, and validated by fitting with the theoretical curves obtained from Eq. (12) (Fig. 7). The optimal constant values are listed in Table 3.

The presence of *form I* seed crystals in the raw mixture had a critical importance for the initiation of phase transition, but there was no effect from increased initial ratio of *form I* to *form III*. The transition at 95 °C stopped at the amorphous phase. Increased amounts of *form I* crystals in raw mixtures decreased the amount of the amorphous phase, which would not readily convert to *form I*.

Similarly, the phase transition kinetics from the amorphous phase to *form I* was investigated at 95 °C, while varying the initial weight fractions of *form I* from 1% to 60% (see Fig. 8).

Table 4
Optimized constant values of amorphous phase and *form I* phase transition kinetics curves at 95 °C.

ω_I in the raw mixture	k', h^{-1}	ω_{A_∞}	q	p
0.01	1.59	0.39	2.05	0.67
0.03	0.96	0.20	1.86	0.67
0.1	1.15	0.19	1.78	0.67
0.2	0.57	0.22	1.39	0.67
0.3	0.93	0.27	1.54	0.67
0.5	0.55	0.12	1.18	0.67
0.6	1.14	0.19	1.40	0.67

3.2.3. The kinetic model of the amorphous phase transition to form I

The phase transition kinetic model of the amorphous phase and *form I* can be expressed (12):

$$\frac{d\omega_I}{dt} = k'\omega_I^p(1 - \omega_I - \omega_{A_\infty})^q \quad (12)$$

The decrease of the amorphous phase with time can be calculated by using Eq. (13):

$$\frac{d\omega_A}{dt} = -k'(1 - \omega_A)^p(\omega_A - \omega_{A_\infty})^q \quad (13)$$

where ω_I is the weight fraction of *form I* at time t; ω_A is the weight fraction of the amorphous phase at time t; ω_{A_∞} is the weight fraction of the amorphous phase when the phase transition has ceased; k' is the phase transition rate constant when the amorphous phase transforms to *form I*; t is the time, h; q, p are the constants; k', ω_{A_∞}, p, q are the optimized values.

The optimal values of the constants obtained by fitting the experimental data with theoretical curves are summarized in Table 4.

Upon heating we observed that the amorphous phase changed into an inactive amorphous phase, which did not further transform into a crystalline form. Furthermore, the longer the samples were heated, the more of the inactive amorphous phase was formed, and the lower was the degree of the amorphous phase conversion to *form I*.

The phase transition rate and the degree of conversion were influenced by the amount of *form I* seed crystals in the raw mixtures. As seed crystals of *form I increased*, the higher the rate and the degree of conversion. Therefore we could not compare the determined phase transition rate constants in those experiments with a different amount of *form I* seed crystals, because the phase transition rate constants may be higher in the experiments where transition levels were low than those with high transition levels. For example, as shown in Table 4, for the mixtures initially containing a 1% weight fraction of *form I*, the phase transition rate constant, k' was 1.59 h^{-1} and the degree of conversion was 61%, while for the

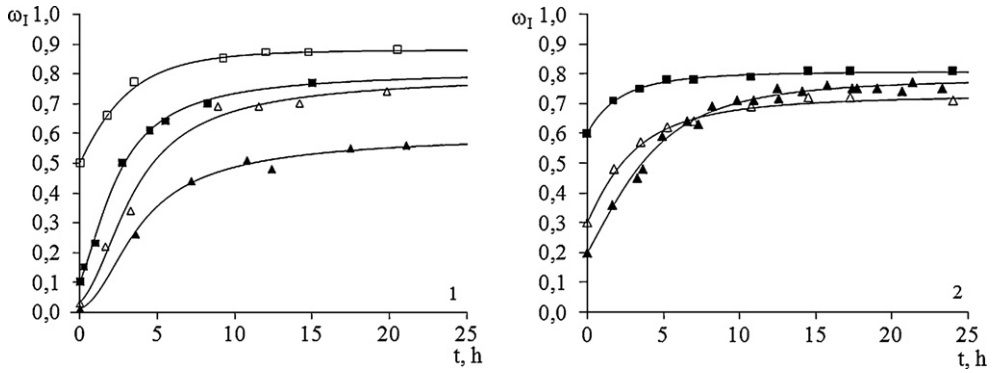

Fig. 8. The phase transition kinetic curves of the amorphous phase and *form I* at 95 °C with 1% (▲), 3% (△), 10% (■), 50% (□) weight fraction of *form I* seed crystals in the raw mixture (1) and 20% (▲), 30% (△), 60% (□) weight fraction of *form I* seed crystals in the raw mixture (2).

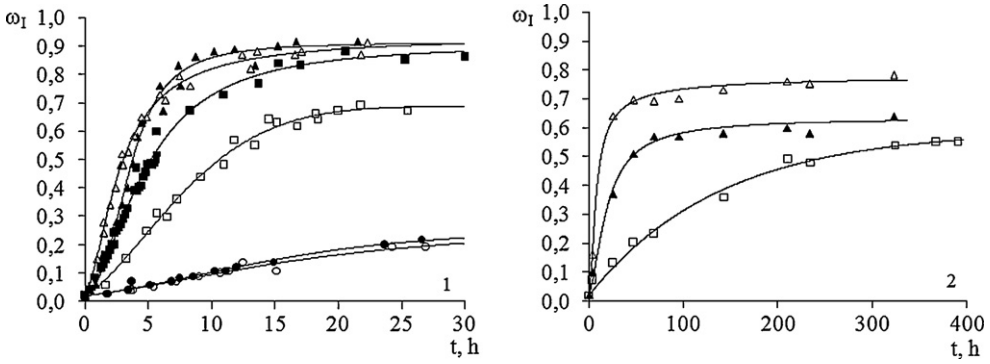

Fig. 9. The phase transition kinetic curves of the amorphous phase and *form I* at 95 °C with 2% weight fraction of *form I* seed crystals in the raw mixture: samples were homogenized by grinding for 1.0 min (□), 1.5 min (■), 2.5 min (△), 5 min (▲); samples were homogenized by shaking for 2.0 min (○), 5.0 min (●) (1); phase transition kinetic curves of the amorphous phase and *form I* at 50 °C under 100% (△), 95% (▲) and 83% (□) RH with 2% weight fraction of *form I* seed crystals in the raw mixture (2).

Table 5
Optimized constant values of amorphous phase and *form I* phase transition kinetic curves at 95 °C containing 2% weight fraction of *form I* seed crystals in the raw mixture: samples homogenized by grinding for 1.0, 1.5, 2.5, 5.0 min and by shaking for 2.0, 5.0 min.

The sample homogenization way	k', h^{-1}	ω_{A_∞}	q	p
Ground for 1.0 min	0.42	0.29	1.30	0.67
Ground for 1.5 min	0.40	0.10	1.48	0.50
Ground for 2.5 min	1.09	0.04	2.18	0.67
Ground for 5.0 min	0.64	0.09	1.07	0.67
Shaken for 2.0 min	0.29	0.75	1.24	0.55
Shaken for 5.0 min	0.24	0.75	0.96	0.59

Table 6
Optimized constants values of amorphous phase and *form I* at 50 °C under high humidity conditions containing 2% weight fraction of *form I* seed crystals in the raw mixture.

RH, %	k', h^{-1}	ω_{A_∞}	q	p
100	0.34	0.23	2.00	0.50
95	0.18	0.36	1.82	0.50
83	0.0072	0.41	1.00	0.50

3% initial weight fraction of *form I* we observed the phase transition rate constant, $k' = 0.96\ h^{-1}$ and an 80% degree of conversion.

The sample preparation method had a significant effect on the observed phase transition rate constants. Grinding a 98:2 mixture of the amorphous phase and *form I* in a mortar and further heating the material for about 30 h at 95 °C resulted in a rapid phase transition and 80–90% conversion. Sample homogenization by shaking a similar amount of the same mixture and further heating the material for about 60 h at 95 °C resulted in less than 25% conversion. The explanation could be that static charge was formed, and the particles formed kinetically stable agglomerates (see Fig. 9-1). The optimal time for the CDCA sample grinding was determined to be 2.5 min. By grinding the sample for 1.0 min, the phase transition was slower, and the conversion of the amorphous phase was 70%. The optimized constants are shown in Table 5.

The amorphous phase transition to *form I* was investigated under high relative humidity (RH) and also at temperatures lower than 80 °C. The rate constants showed a dependence on RH; with significantly increased rates as RH increased. That is shown in Fig. 9-2, with the examples of the amorphous phase transition to *form I* at 50 °C under 100%, 95% and 83% RH. We observed a significantly slower phase transition at 50 °C and 74% RH (Table 6).

Combining the Runge–Kutta differential equation solving method with the multi-point optimization method for phase transition curve modeling of CDCA polymorphs, the average quadratic deviation of the acquired experimental results from one calculated series was under 2%.

4. Conclusions

When examining the phase transition of CDCA from *form III* to *form I* at high temperature conditions, it was determined that *form III* amorphized without the presence of *form I* nuclei, and the activation energy of this kinetic process was 210 kJ/mol. The spontaneous formation of *form I* at experimental circumstances was not established, and seed crystals were necessary for obtaining *form I*. A kinetic model was created to describe the *form I* crystal growth, including seed crystal growth in three-dimensions, the phase transition rate proportionality to the surface area of *form I* crystals and the influence of the amorphous phase surface area changes with an empirical stage pointer q that accounts for the incomplete transition of the amorphous phase to *form I* with a residue ω_{A_∞}. Such a phase transition is described by an analytically intractable differential equation:

$$\frac{d\omega_I}{dt} = k_2\omega_I^p(1 - \omega_{III} - \omega_I - \omega_A^\infty)^q$$

The degree of conversion and the phase transition rate constant depended on the quantity of *form I* nuclei in the raw mixture and on the sample preparation. To describe the phase transition kinetic curves, the Runge–Kutta differential equations were solved numerically. By combining the Runge–Kutta differential equation solving method with the multi-point optimization method, the average quadratic deviation of the experimental results from the calculation was under 2%. The novel kinetic model can be used for the determination of thermodynamic stability regions of pharmaceutically active substances to ensure a safe storage of drug products.

References

[1] S.R. Vippagunta, H.G. Brittain, D.J.W. Grant, Crystalline solids, Drug Deliv. Rev. 48 (2001) 3–26.
[2] F. Kato, M. Otsuka, Y. Matsuda, Kinetic study of the transformation of mefenamic acid polymorphs in various solvents and under high humidity conditions, Int. J. Pharm. 321 (2006) 18–26.
[3] Z. Nemet, G. Csonka Kis, G. Pokol, A. Demeter, Quantitative determination of famotidine polymorphs: X-ray powder diffractometric and Raman spectrometric study, J. Pharm. Biomed. Anal. 49 (2009) 338–346.
[4] T. Oguchi, N. Sasaki, T. Hara, Y. Tozuka, K. Yamamoto, Differentiated thermal crystallization from amorphous chenodeoxycholic acid between the ground specimens derived from the polymorphs, Int. J. Pharm. 253 (2003) 81–88.
[5] G. Guiseppetti, M. Paciotti, Polymorphism of chenodeoxycholic acid, Farmaco Educ. Sci. 33 (1978) 64–72.
[6] M. Alvarez, A. Jover, J. Carrazana, F. Meijide, V.H. Soto, J. Vazquez Tato, Crystal structure of chenodeoxycholic acid, ursodeoxycholic acid and their two 3β,7α- and 3β,7β-dihydroxy epimers, Steroids 72 (2007) 535–544.
[7] G.A. Stephenson, J.G. Stowell, P.H. Toma, D.E. Dorman, J.R. Greene, S.R. Byrn, Solid-state analysis of polymorphic, isomorphic, and solvated forms of dirithromycin, J. Am. Chem. Soc. 116 (1994) 5766–5773.
[8] P.F. Lindley, M.M. Mahmoud, F.E. Watson, W.A. Jones, The structure of chenodeoxycholic acid, C24H4004, Acta Cryst. B36 (1980) 1893–1897.

[9] P.J. Rizkallah, M.M. Harding, P.F. Lindley, A. Aigner, A. Bauer, Structure of a low-temperature polymorph of chenodeoxycholic acid, $C_{24}H_{40}O_4$, determined with synchrotron radiation, Acta Crystallogr. B46 (1990) 262–266.
[10] G.A. Stephenson, R.A. Forbes, S.M. Reutzel-Edens, Characterization of the solid state: quantitative issues, Adv. Drug Deliv. Rev. 48 (2001) 67–90.
[11] S.N. Campbell Roberts, A.C. Williams, I.M. Grimsey, S.W. Booth, Quantitative analysis of mannitol polymorphs. X-ray powder diffractometry-exploring preferred orientation effects, J. Pharm. Biomed. Anal. 28 (2002) 1149–1159.
[12] H. Zhu, J. Xu, P. Varlashkin, S. Long, C. Kidd, Dehydration, hydration behavior, and structural analysis of fenoprofen calcium, J. Pharm. Sci. 90 (2000) 845–859.
[13] K. Urakami, A.E. Beezer, A kinetic and thermodynamic study of seratrodast polymorphic transition by isothermal microcalorimetry, Int. J. Pharm. 257 (2003) 265–271.
[14] J. Huberty, H. Xu, Kinetic study on phase transformation from titania polymorph brookite to rutile, J. Solid State Chem. 181 (2008) 508–514.